Integrated Ray Tracing (IRT) simulation of SCOTS surface measurement of GMT Fast Steering Mirror Prototype

Ji Nyeong Choi[*a,b], Dongok Ryu[a,b], Sug-Whan Kim[a,b,c], Logan Graves[d], Peng Su[d], Run Huang[d], Dae Wook Kim[d]

[a]Space Optics Laboratory, Dept. of Astronomy, Yonsei University, Republic of Korea; [b]Center for Galaxy Evolution Research, Yonsei University, Republic of Korea; [c]Yonsei University Observatory, Yonsei University, Republic of Korea; [d]College of Optical Science, The University of Arizona, Tucson, Arizona 85721, USA

ABSTRACT

The Software Configurable Optical Testing System (SCOTS) is one of the newest testing methods for large mirror surfaces. The Integrated Ray Tracing (IRT) technique can be applicable to the SCOTS simulation by performing non-sequential ray tracing from the screen to the camera detector in the real scale. Therefore, the radiometry of distorted pattern images are numerically estimated by the IRT simulation module. In this study, we construct an IRT SCOTS simulation model for the Fast Steering Mirror Prototype (FSMP) surface of the Giant Magellan Telescope (GMT). GMT FSMP is an off-axis ellipsoidal concave mirror that is 1064 mm in diameter and has PV 3.1 mm in aspheric departure. The surface error requirement is less than 20 nm rms. The screen is modeled as an array of 1366 by 768 screen pixels of 0.227 mm in pitch size. The screen is considered as a Lambertian scattering surface. The screen and the camera are positioned around 4390 mm away from the mirror and separated by around 132 mm from each other. The light source are scanning lines and sinusoidal patterns generated by 616,050 rays per one screen pixel. Of the initially generated rays, 0.22 % are received by the camera's detector and contribute to form distorted pattern images. These images are converted to the slope and height maps of the mirror surface. The final result for the height difference between input surface and reconstructed surface was 14.14 nm rms. Additionally, the simulated mirror pattern image was compared with the real SCOTS test for the GMT FSMP. This study shows applicability of using the IRT model to SCOTS simulation with nanometer level numerical accuracy.

Keywords: Optical Testing; Deflectometry; Integrated Ray Tracing

1. INTRODUCTION

An essential characteristic for developing next generation's ground based astronomical telescopes is an ever larger collecting area for the mirror. Typically segmented mirrors are used for large telescope systems with a collecting area exceeding ten meters. Two notable segmented mirror designs include the 492 1.4 m segmented mirrors design for the 30.0 m primary mirror in Thirty Meter Telescope (TMT) [1] and the 984 1.45 m segmented mirrors making up the 39.1 m primary mirror in European Extremely Large Telescope (E-ELT) [2]. The large number of segmented mirrors implies that massive productivity of mirrors with 1~2 m diameter is strongly related to cost for developing large telescopes as we mentioned above. Following that, the speed and accuracy of mirror surface testing for examining surface condition during mirror fabrication becomes a critical issue.

There are several traditional methods for reflective surface measurement, including the Coordinate Measuring Machine (CMM), the touching or optical profilometer, and Computer Generated Hologram (CGH) interferometry [3]. In this paper, we deal with another method, Phase Measuring Deflectometry (PMD). The PMD test setup consists of an LCD screen with an illuminating pattern and a camera. The pattern is reflected from the surface mirror and the distorted image is captured by the PMD [4]. Through pattern image analysis, the slope of the mirror surface is derived. The application of the law of reflection is a basic operating principle in PMD. The Software Configurable Optical Testing System (SCOTS), a PMD application, has been designed and applied to the surface shape measurement of meter-level mirrors and achieved

*dorothycjn@galaxy.yonsei.ac.kr; phone 821072714742

nanometer level accuracy, comparable to the quality of interferometry [5], [6]. In addition, SCOTS is suitable to measure aspheric surfaces due to the large dynamic range of the measurable surface shape. Lastly, any auxiliary optics are needless in most SCOTS aspheric surface tests, unlike interferometry which can require expensive null optics.

In this study, the objective target for the SCOTS test is the GMT Fast Steering Mirror Prototype (FSMP). The GMT FSM is a segmented secondary mirror system. The prototype of GMT FSM (FSMP) has been fabricated and polished [7]. The GMT FSMP has an off-axis aspheric surface; the full detailed specification for the mirror are provided in Table 1 [8]. For the GMT FSMP surface test both CGH interferometery as well as SCOTS were applied. This provides a great advantage, as both methods are verified by each other, and both methods rely on a fundamentally different physical principle.

Table 1. Specification of GMT FSMP surface shape.

Item	Value	Remarks
Diameter	1064.000 mm	3.2 m in secondary mirror assembly
Off-axis distance	1088.900 mm	Except center part
Radius of curvature	4166.747 mm	Concave
Conic constant	-0.7154	Ellipsoid

There are several error sources which contribute to the uncertainty in the surface measurement of SCOTS. In order to enhance measurement accuracy, all suspicious error sources should be analyzed and calibrated by extra test processes. For example, the position error of camera and screen, one of the major error sources in the SCOTS test, is well-calibrated by multiple position measurements by a laser tracker [6]. In addition, non-geometric error sources, such as the camera's stray light or the screen illumination uniformity, also cause measurement uncertainty. These factors are closely related to radiometric performance in the SCOTS test. Finally, it is necessary to estimate the irradiance distribution of distorted pattern images on the camera detector where experimental raw data is generated.

An Integrated Ray Tracing (IRT) simulation can be a good solution for simulation of the camera's image. IRT has been applied to simulate end-to-end performance of an optical system, including astronomical telescopes, in a real environment [9]. IRT performs non-sequential ray tracing in the system, incorporating models of light source, medium, target and observing instruments in real scale with realistic optical properties. Like the preceding, we can develop the IRT simulation model of a SCOTS mirror test, and then estimate radiometric performance on the SCOTS camera detector. It can provide excellent calibration for the system for non-geometric error sources which could otherwise not be measured quantitatively.

In this study, we simulate the SCOTS test for the GMT FSMP with an IRT simulation method. We describe the IRT model for SCOTS and the result of the simulation and discuss what they mean. In Section 2, the IRT simulation model for SCOTS and image analysis for surface reconstruction are described. The result of surface reconstruction and distorted pattern image comparison between simulation and experiment are reported in Section 3. This is followed by the discussions on the factors influencing simulation errors in Section 4, before the concluding remarks in Section 5.

2. METHODOLOGY

2.1 IRT Simulation Model for SCOTS Test

We developed an IRT simulation model of the SCOTS test for the GMT FSMP. We used Breault Research Organization's Advanced Systems Analysis Program (ASAP®) as a non-sequential ray tracing engine. We built the simulation model of each SCOTS component; screen, mirror and camera. The position of each component is defined by laser tracker coordinate data. Four reference points of each component were measured by a laser tracker with Spherical Mounted Retroreflectors (SMR) and converted to the center position and attitude in a global coordinate system. The reference of the global coordinate system was defined as the center of mirror surface. Three reference axis were defined to be parallel to the mirror's local coordinate axes. As a result, the distance between mirror and the SCOTS module was calculated to be around 4390 mm. Also, the camera and screen were separated by approximately 132 mm in the X-axis direction. Figure 1 shows a schematic diagram of the SCOTS test system for the GMT FSMP. Also, Figure 2 shows the ASAP® simulation model of the SCOTS components with traced rays.
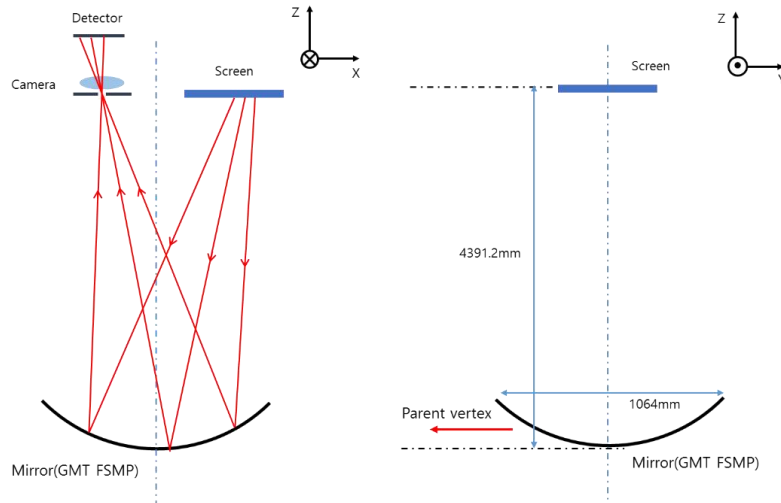
Figure 1. Schematic diagram of SCOTS for GMT FSMP surface test
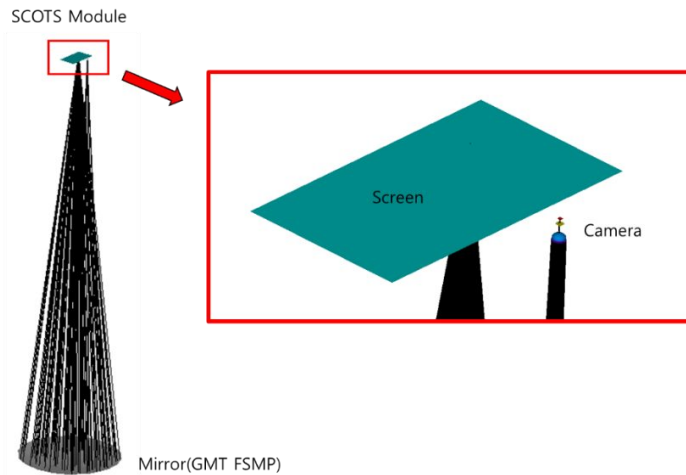
Figure 2. ASAP® simulation model of SCOTS with traced rays (black lines). Only one thousand rays are represented for visualization purpose.

The measurement target was the GMT FSMP, an off-axis aspherical surface. We substituted the value of the diameter, curvature, conic constant and off-axis distance from Table 1. In addition to the ideal surface figure, a measured surface irregularity, 0.211 μm rms surface error, was added to the simulated mirror surface model. The surface error was represented by 37 Zernike fringe polynomial terms, excluding the 1~4 terms. The value of the surface error was derived from the real SCOTS test data of the GMT FSMP. The Zernike polynomial coefficients of the input surface error were compared to the value of reconstructed surface error in Section 3.1. The reflectivity of the mirror surface was assumed to be 1.0 without any light scattering.

The LCD panel, composed of an array of 1366 by 768 pixels, of which pitch the size was 0.227 mm, was used in the real SCOTS test for the GMT FSMP. In the IRT simulation, only 291 by 275 screen pixels, the minimum coverage area for all mirror surface illumination, were used in the ray tracing to reduce the simulation run time. A total of 616,050 rays were used to simulate a single screen pixel's illumination. Rays are initially launched behind the screen plane. As the rays propagate through the screen, scattered rays are generated as shown in Figure 3. To enhance the computational efficiency

of the massive numerical ray tracing, the scattering ray angles were limited within the solid angle covering the FSMP surface. Finally, only 0.22% of the initial rays traced participate in pattern image formation.
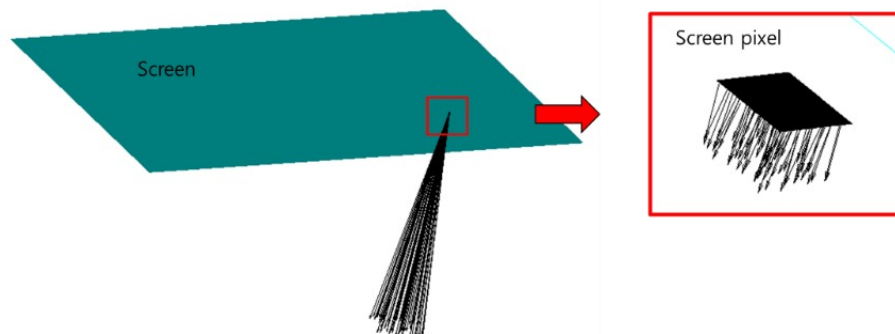
Figure 3. ASAP® simulation model of SCOTS screen. Rays (black lines) are generated and propagated from a screen pixel. Only one thousand rays are represented for visualization purpose.

The SCOTS camera was designed with a 15 mm focal length and 1 mm diameter entrance pupil. Figure 4 shows the ASAP® simulation model of the camera's optical system, including an aspherical plano lens with a 1 mm diameter iris and camera detector with window. Although the optical properties of the window cause it to filter light in the IR, we did not adjust for the optical properties related to wavelength dependence because only a single wavelength, 587.6 nm, was used in this simulation. While the actual detector used in the GMT FSMP SCOTS test consists of 1384 by 1032 pixels with a 4.65 μm pitch size, in order to improve the numerical efficiency and accuracy, we combined 8 pixels to a single pixel (i.e. data binning) and cut the dark boundary. Finally, the simulation model of the camera detector was defined as 101 by 101 pixels with a 37 μm pitch size.
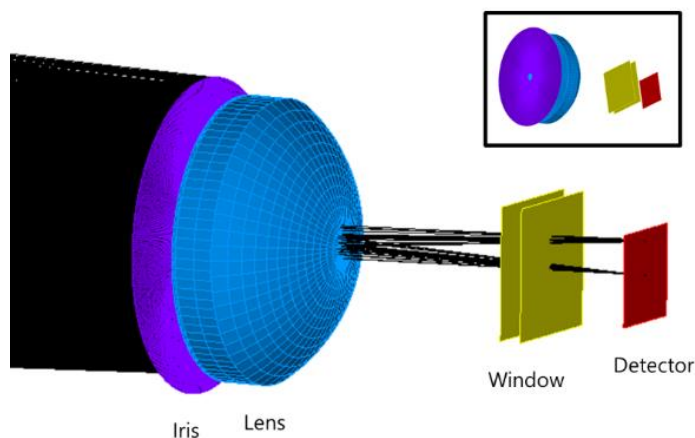
Figure 4. ASAP® simulation model of camera optical system with traced rays (black lines).

One of the advantages of the IRT simulation is simultaneous calculation of imaging and radiometric performance. Rays are generated and propagated while performing a radiometric transfer calculation of each ray. In this SCOTS IRT simulation case, the radiant power of each ray arriving at the detector (f_d) is calculated according to equation (1)

$$f_d = f_i \cdot BSDF(\theta_s, \varphi_s) \cdot R_{mirror} \cdot T_{optics} \qquad (1)$$

f_i denotes incident ray radiant power; $BSDF(\theta_s, \varphi_s)$ is Bidirectional Scattering Distribution Function of each scattering angle θ_s, φ_s; R_{mirror} is the reflectance of the mirror surface; and T_{optics} denotes the transmittance of the camera. BSDF is constant with scattered angle because the screen pixel's illumination was assumed to be Lambertian scattering. Additionally, reflectance of the mirror surface and transmittance of the camera were both assumed to be 1.0. Finally, the irradiance distribution on the camera detector was numerically derived from radiant power integration of rays on each detector pixel's area.

2.2 Image Analysis for Surface Reconstruction

Figure 5 illustrates the integration of images from a single pixel's illumination to make a line pattern or sinusoidal pattern image. We firstly generated 291 by 275 images of each single pixel's illumination. Then we composed 291 X-axis line scan images and 275 Y-axis line scan images by image summation of each screen pixel forming each line. Although the screen's illumination pattern is a line, a ring shaped line (which includes the surface slope information) appeared on the detecting image as shown in Figure 5(b). Similarly, sinusoidal pattern images were derived from a sinusoidal valued-weighted sum of line pattern images.

(a)   (b)   (c)
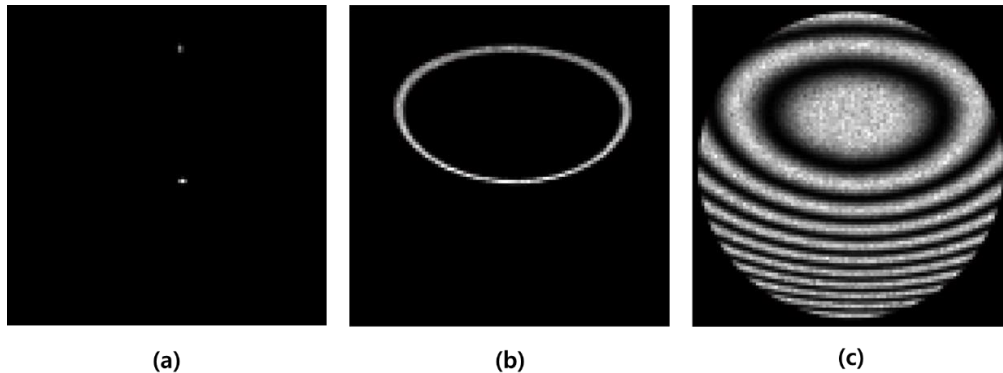
Figure 5. (a) A unit image generated by one screen pixel illumination. (b) A distorted line pattern image from 27th Y-axis scan line on the screen. (c)The total mirror image generated by sinusoidal pattern illumination on the screen.

As a real camera lens was included into the IRT simulation model, camera distortion was also corrected to know the exact surface area shown by each camera detector pixel by performing ray tracing from each camera detector pixel to the mirror. 100 rays were used to reverse ray trace from each detector pixel to the mirror surface through the camera lens and aperture. The centroid value was then derived from the rays' destination coordinates on the mirror surface and was matched to the corresponding detector pixel.

Distorted pattern images can be converted to mirror surface height by integrating the slope of the surface, which in turn can be calculated based on the law of reflection. The coordinates of camera aperture center, specific mirror and screen point matched with each detector pixel are input values of the surface slope equation [5]. Mirror points were matched to each detector pixel by camera distortion correction, as mentioned previously. Screen points are derived by centroid calculation of line pattern images, such as the one shown in Figure 5(b), or with the phase shifting method with sinusoidal pattern images, as shown in Figure 5(c) [5]. Finally, surface slopes in two orthogonal directions are calculated and also

converted to surface height by zonal estimation or model estimation [10]. In Section 3, we will present the reconstructed mirror surface derived from the SCOTS IRT simulation. Additionally, simulated pattern images will be compared to the pattern images from the real SCOTS test of the GMT FSMP.

3. RESULT

3.1 Surface Reconstruction

Figure 6 shows reconstructed surface slopes and height derived from the SCOTS IRT simulation image analysis we described in Section 2. The area of more than 95% of the mirror diameter (1010.8 mm) was masked because zonal estimation, used in slope to height conversion, has intrinsic error at the boundary of the mirror image. Surface error was extracted by subtracting the ideal conical surface from the reconstructed surface. Figure 7 shows the reconstructed surface error and the difference between input and reconstructed surface error. The difference, which gives the accuracy of the SCOTS IRT simulation for the GMT FSMP, was 14.14 nm rms and had a uniformly random noise pattern. The IRT simulation error in surface reconstruction will be discussed in Section 4.
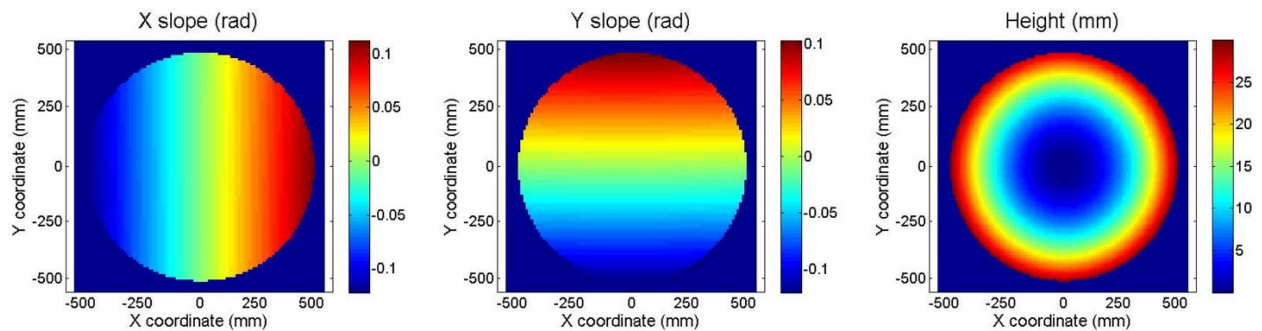
Figure 6. 2D maps of surface slopes in X and Y-axes and surface height derived from SCOTS IRT simulation image analysis.
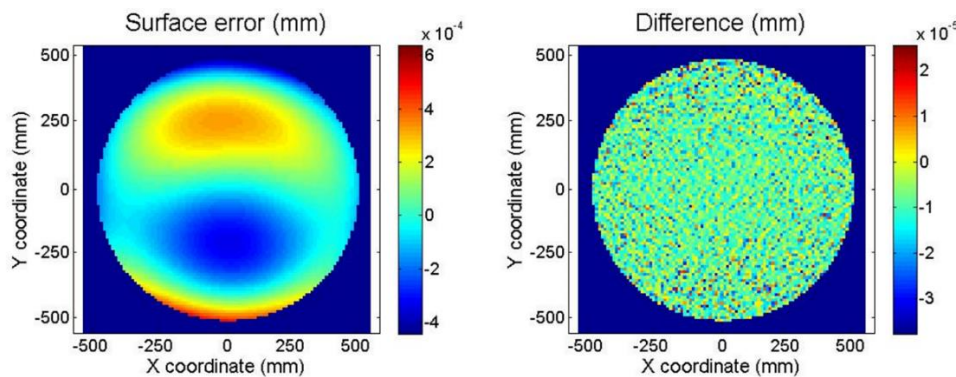
Figure 7. 2D maps of reconstructed surface error (left, 0.211 μm rms) and difference between input and reconstructed surface error (right, 14.14 nm rms).

Surface error can be expressed by Zernike polynomial terms. Surface error was fitted with 37 Zernike fringe polynomial terms, excluding the first 1 ~ 4 terms. Figure 8 shows the values of Zernike polynomial coefficients representing input surface error and the differences between input and reconstructed Zernike polynomial coefficients. The X-axis denotes the order of Zernike polynomial terms from 5 to 37 and the Y-axis denotes the value of the coefficient. As shown in Figure 7, the input surface had a large coma component in the Y direction (i.e. the 8th Zernike polynomial term). The coefficient

differences between input and reconstructed surface error are all less than 0.1%. Relatively higher difference values occurred in the 9 (primary spherical), 16 (secondary spherical), 25 (tertiary spherical), 36 and 37 (higher order spherical) Zernike terms. Additional work is needed to understand the property of reconstruction error related to radial Zernike polynomial terms.
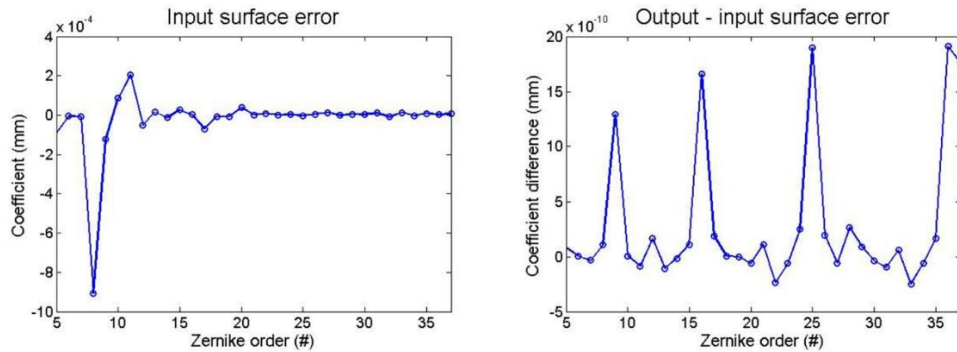
Figure 8. Plots of Zernike polynomial (fringe) coefficient of input surface error (left) and differences of coefficients between input and output surface error (right).

3.2 SCOTS Camera Image Simulation
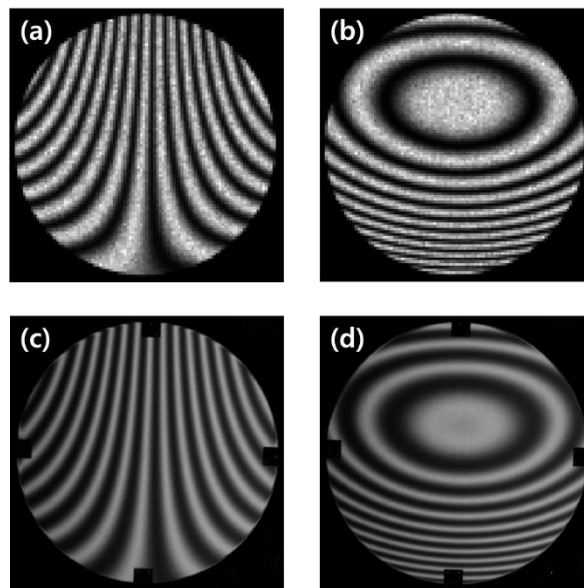
Figure 9. Sinusoidal pattern images captured by camera detector. (a) and (b) are SCOTS IRT simulation images, (c) and (d) are snapshots of GMT FSMP SCOTS test.

As described in Section 2, the radiometric performance is simultaneously calculated with distorted pattern images formed on the camera detector by using an IRT simulation model. Figure 9 shows the comparison of sinusoidal pattern images from the simulation and real test. Figure 9(c) and (d) are raw image data, which were taken from the GMT FSMP SCOTS test performed in March, 2014 [7]. Black square patches located in the boundary of real test mirror image are caused by an obscuration from the SMR's jig structure. Although the quality of simulated images are worse than the real test data due to pixel binning and image fluctuation caused by ray deficiency (i.e. numerically insufficient number of rays), the

pattern shape on both images are extremely similar. The trivial difference in pattern shape seems to be mainly caused by geometric discrepancy between the simulation and the real test. For instance, there are some uncertainties in the process of distance measurements using laser trackers. If the geometric uncertainties are all well-corrected, image differences can only be seen by image subtraction. Then, it will be closely related to non-geometric error sources; for example, the stray light effect in the camera.

4. DISCUSSION

The number of rays participating the ray tracing is one of the major factors causing the simulation's computation error, by generating image fluctuation. The image fluctuation noise can be estimated from images generated from the same ray number but varied by a random seed. We calculated standard deviation of each detector pixel's irradiance derived from 10 identical images with different random distributions for the ray. In the case of 616,050 rays per screen pixel, the standard deviation of pixel irradiance was 8.30 %. Then, the precision of surface reconstruction was derived to 9.82 nm. As the number of rays are increased, simulation error will decrease.

However, we also should consider simulation run time. It takes longer to perform the simulation as the number of rays is increased, although simulation error is getting smaller. Therefore, the appropriate ray number should be determined, while considering the requirement of simulation accuracy and the duration of the simulation, given the computer's specific performance capabilities. In this case with the ray number we mentioned above, it took around 4 days to complete the ray tracing with a single core, Intel Core i7 CPU running at 3.40 GHz. We can reduce run time by using a multi-core CPU. (As an example, the same simulation including all the ray tracing process can be completed in a day using a 4 multi-core CPU.)

5. CONCLUSION

We developed an IRT simulation module for the GMT FSMP SCOTS test. We simulated pattern images formed by rays from the mirror surface reflection. After image analysis for surface reconstruction, the accuracy of the IRT simulation with the given ray number is derived to nanometer level. Moreover, we compared images from the IRT simulation and real SCOTS test for the GMT FSMP. When developing the IRT simulation model for SCOTS, we contributed to the calibration of the SCOTS system, providing simulation test results of the SCOTS test including various error sources. According to the IRT simulation model, it is possible to perform error analysis while considering not only geometric but also non-geometric error sources, such as stray light. We will report the IRT simulation error analysis results as following research. Finally, IRT simulations of the SCOTS test are expected to play an important role in future mirror tests, and massive mirror production for large mirror telescope development.

REFERENCES

[1] Nelson, J. and Sanders, G. H., "The status of the Thirty Meter Telescope project," Proc. SPIE 7012, 70121A (2008).
[2] McPherson, A., et al. "Recent progress towards the European extremely large telescope (E-ELT)," The Messenger 148, 1-8 (2012).
[3] Valente, M., Lewis, B., Melena, N., Smith, M., Burge, J. H., Zhao, C., "Advanced surface metrology for meter-class optics," Proc. SPIE 8838, 88380F (2013).
[4] Knauer, M. C., Kaminski, J., Hausler, G., "Phase measuring deflectometry: a new approach to measure specular free-form surfaces," Proc. SPIE 5457, 366 (2004).
[5] Su, P., Parks, R. E., Wang, L. et al., "Software configurable optical test system: a computerized reverse Hartmann test," Appl. Opt. 49, 4404-4412 (2010).
[6] Su, P., Wang, S., Khreishi, M., Wang, Y., et al., "SCOTS: a reverse Hartmann test with high dynamic range for Giant Magellan Telescope primary mirror segments," Proc. SPIE 8450 (2012).
[7] Cho, M., Corredor, A., Cribusch, C., et al., "Development of GMT fast steering secondary mirror assembly," SPIE Astronomical Telescopes+ Instrumentation, 91451M (2014).
[8] Kim, Y.-S., Ahn, K. B., Park, K., Moon, I. K., and Yang, H. S., "Accuracy assessment for measuring surface figures of large aspheric mirrors," Journal of the Optical Society of Korea 13, 12 (2), 178-183 (2009).
[9] Breault, R. P., Kim, S. W., Yang, S. K., Ryu, D., "Sun-, Earth- and Moon-integrated simulation ray tracing for observation from space using ASAP," Proc. SPIE 9189, 91890F (2014).
[10] Southwell, W. H., "Wave-front estimation from wave-front slope measurements," J. Opt. Soc. Am. 70, 998-1006 (1980)